How reference electrodes improve our understanding of degradation processes in half and full cell potassium-ion battery setups

Iurii Panasenko [ID], Monika Bäuerle , Fabian Jeschull [*] [ID]

Karlsruhe Institute of Technology (KIT), Institute for Applied Materials – Energy Storage Systems (IAM-ESS), Hermann-von-Helmholtz-Platz 1, 76344 Eggenstein-Leopoldshafen, Germany

ARTICLE INFO

ABSTRACT

Electrochemical testing of electrodes for K-ion batteries (KIBs) can be strongly affected by interferences from electrolyte degradation reactions and associated crosstalk. This affects half cell measurements in particular. To address this issue, inert and stable reference electrodes are required for reliable 3-electrode measurements that allow to distinguish reversible electrochemical electrode processes more clearly from irreversible parasitic reactions. Therefore, this study evaluated K-metal and a partly charged positive electrode ($K_2Fe[Fe(CN)_6]$, KFF), as two established solutions from the Li-ion battery field. Their electrochemical stability and suitability in various 3-electrode cell setups are evaluated in half and full cell, as well as symmetric cell configurations. Our experiments revealed that the high reactivity of the K-metal as reference or counter electrode interferes considerably with the electrode processes, leading to additional features in the voltage profile of KFF. Furthermore, any amount of K-metal led to a crosstalk-induced self-discharge of KFF. This places considerable limitations on the materials that can be used as a reference electrode. Therefore, we introduced an alternative reference electrode based on Ag/AgCl in a separate cell compartment, with high flexibility in the choice of the electrolyte formulation. To demonstrate the efficacy of this approach, we examine the impact of the electrolyte additive 1,3,2-dioxathiolane 2,2-dioxide (DTD) in 3-electrode setups, with the aim to illustrate the influence of DTD on the electrochemical processes of K-metal, KFF, and graphite electrodes in different cell configurations.

1. Introduction

The majority of electrochemical electrode testing is traditionally conducted in so-called half cell configurations, where a metal foil serves as counter electrode (CE), i.e. in alkali-ion cells metallic lithium (Li), sodium (Na) or potassium (K). Recent studies show that this cell configurations bear a lot of issues in post-Li systems, in particular K-ion batteries (KIBs), due to the extensive side reactions at the highly reactive metallic CE. Several groups demonstrated in recent studies using gas chromatography [1–3] and highly surface sensitive X-ray photoelectron spectroscopy [2,4,5] that severe degrees of electrode crosstalk through electrolyte degradation products and considerable amounts of surface deposits evolve rapidly in potassium cell systems. These (mostly) chemical processes can interfere significantly with electrochemical processes leading to high cell resistances [6], voltage hysteresis [7] or misleading voltage signatures and potential drifts during cycling.

This raises issues, especially in 2-electrode (2e) half cell setups, where the K-metal CE (K-CE) acts as a quasi-reference (QRE) or counter-

reference electrode, as its surface chemistry and electrochemical behaviour has adverse impact on the working electrode. To address this problem, more experiments in full cell configurations [8–10] i.e. in absence of metallic potassium, and in 3-electrode (3e) cell configurations would be needed [3]. In 3e cells the CE and WE potentials can be controlled and recorded separately which would help greatly in distinguishing reversible electrochemical processes more clearly from irreversible ones and the ones that are only associated with parasitic reactions at the K-CE. To this end, due to the lack of alternatives and out of convenience the alkali metals also frequently serve as reference electrodes (RE) in 3e cell configurations[11–13], which pose potentially similar shortcomings for the reasons stated above.

The assumption for alkali metal-based QREs and REs is that the bulk electrode's activity and potential will practically not change over the course of the experiment if the current density is small. The prefix 'quasi' (or 'pseudo') is added to suggest that the electrode is not in a true thermodynamic equilibrium with its oxidized species in solution (i.e. the cations in the electrolyte). In the case oxidized surface compounds are

---

* Corresponding author.
  E-mail address: fabian.jeschull@kit.edu (F. Jeschull).

formed at the electrode surface, e.g. a Ag_2O film on Ag wire or the solid electrolyte interface (SEI) on K-metal, the cation concentration is never known exactly and are also subjected to time-dependent changes. According to Nernst equation, this inevitably leads to a drift in potential, for instance when the layer dissolves or grows. In order to mitigate the ongoing side reactions at the K-metal electrode Komaba and coworkers proposed to passivate the electrode as a pretreatment in a carbonate-based electrolyte with high concentrations of potassium bis(fluorosulfonyl)imide (KFSI) [13]. More universal RE approaches from other monovalent battery chemistries include silver-based REs [14], alloys [15–18] and partially charged electrode materials [19]. For KIBs, however, there is still a knowledge gap on the topic of reliable REs, which is associated with challenges of integrating REs into thin layer battery setups like coin or pouch cells with limited electrolyte volumes and general difficulties related to RE stability in non-aqueous electrolytes. The most widely used options in non-aqueous systems are Ag|Ag^+[20–22] REs (e.g. Ag-wire (Ag/Ag_2O) or Ag/$AgNO_3$), but other alternatives, such as Ag|Ag_2S [14] and Ag|AgCl[23], have been reported to offer higher reliability [24]. In recent studies by Lee and Tang[22,25], a non-aqueous Ag|$AgNO_3$ reference electrode was used to highlight the problems of Na-metal electrodes. The authors concluded that the degradation products from Na-metal as reference or counter electrode affect the electrochemistry at the working electrode, due to crosstalk. Clearly, the more reactive post-Li systems benefit from more inert reference electrode to avoid interferences with the electrode reactions.

In the context of this study, the even higher reactivity of K-metal motivates the use of more inert REs, especially if they could be located in a separate electrode compartment. The two main requirements for reference electrodes are that 1) they must be non-polarizable and 2) provide reliable and reproducible potentials [26,27]. The first requirement is fulfilled at small exchange current densities, fast electrode kinetics and high electrode surface areas. However, QRE typically do not fulfil this requirement as their plating/stripping potential is proportional to the applied current density [6]. To ensure a constant potential over time, constant ion activity is necessary, which is challenging to achieve if the surface chemistry is highly dynamic as in the surface layers of alkali metals [2–5] and additionally strongly dependent on the electrolyte formulation [1,13,28].

In this study, we evaluate three different types of REs, namely a K-metal QRE, a partly charged $K_xFe[Fe(CN)_6]$ ('KFF-RE') and a sat. Ag|AgCl RE ('AgCl-RE'), in various 2e and 3e KIB setups in half and full cells. Furthermore, for the integration of the AgCl-RE, a modified cell setup is proposed to one reported previously by Bünzli et al. [12]. The present work thus offers a novel and viable implementation of a silver-based RE in thin layer battery configuration with limited electrolyte volume of 200 μL or less. Our results demonstrate that the high reactivity of K-RE fails to provide reliable results in electrolytes without a passivation additive. It will be shown that the presence of even small amounts of K-metal can have detrimental effects on the electrochemistry of the working electrode. Moreover, a parasitic self-discharge mechanism is described herein that reduces the shelf-life of the Prussian blue analogue (PBA) $K_2Fe[Fe(CN)_6]$ ('KFF') considerably. The AgCl-RE proved to be the most suitable and versatile choice for half and full cell setups, as outlined in the second part of this study, where the AgCl-RE was applied to investigate the impact of the electrolyte additive 1,3,2-dioxathiolane 2,2-dioxide (DTD) on the electrode reactions at the positive and negative electrode in various cell configurations.

2. Experimental section

Materials. Graphite powder (C—NERGY Actilion GHDR 15–4) and carbon black (Super C65) were obtained from Imerys Graphite & Carbon, carboxymethyl cellulose (CMC—Na), and polyacrylic acid (PAA, M_v = 1.250 kg mol^{-1}) was acquired from Merck. Chemicals that used for PBA synthesis: $FeSO_4 \cdot 7H_2O$ (99 %, VWR chemical), polyvinylpyrrolidone (M_w = 40.000, Aldrich), $Na_3Cit \cdot 5.5\ H_2O$ (99.5 %,

Sigma-Aldrich), $K_4Fe(CN)_6 \cdot 3H_2O$ (99 %, Sigma), of PVdF (HSV900, GelonLib), *N*-methyl-2-pyrrolidone (99.5 %, Sigma-Aldrich). Electrolyte solvents and the additive, ethylene carbonate (EC, >99 %, anhydrous, BASF), diethyl carbonate (DEC, Merck, >99 %), propylene carbonate (PC, 99.7 %, Sigma-Aldrich), DTD (98 %, Sigma-Aldrich) and Ferrocene (99.5 %, Alpha Aesar) were used as received. Whatman GF/B separators were dried before use at 120 °C for 12 h under vacuum. Celgard 2325 separators were stored in the glovebox antechamber under vacuum overnight before use. Lithium discs (PI-KEM, purity: 99.9 %, 250 μm thick, 16 mm in diameter) were used as received. Potassium metal (chunks, 98 %, Thermo Scientific) was stored in mineral oil and cleaned in heptane prior to use.

Synthesis of $K_2Fe[Fe(CN)_6]$ (KFF). $K_2Fe[Fe(CN)_6]$ was synthesized via a co-precipitation method [29]. Three solutions were prepared: (a) 0.782 g of $FeSO_4 \cdot 7H_2O$ and 0.100 g of polyvinylpyrrolidone in 20 mL of deionized water, (b) 0.244 g of $Na_3Cit \cdot 5 \cdot 5H_2O$ in 10 mL of deionized water, and (c) 1.268 g of $K_4Fe(CN)_6 \cdot 3H_2O$ in 10 mL of deionized water. The solutions were added to the vessel in the order (a), (b), and (c). The resulting suspension was stirred for 36 h at ambient temperature. Subsequently, the resulting precipitate was centrifuged and washed with a mixture of ethanol and deionized water (1:1 ratio by volume) several times and dried at 150 °C for 12 h under vacuum (10^{-3} mbar). After drying, the obtained powder was ground using a mortar.

Electrode Preparation. In this study both graphite negative electrode and Prussian white positive electrodes were used to outline the issues in combination with different reference electrodes.

Graphite electrodes. The negative electrode consisted of a mixture of graphite, carbon black and a binder mixture of carboxymethyl cellulose and polyacrylic acid binders in a weight ratio 95:1:2:2. The total solid content of the electrode slurry was 1 g. A binder solution was prepared by dissolving CMC—Na (20 mg) in 1 ml of deionized water and mixing for 5 min at 2000 rpm in a Thinky mixer. PAA (20 mg) and 0.5 mL of water were added in the next step and the solution was mixed another 5 min. The resulting 1.5 mL binder solution was blended with 10 mg (of carbon black and mixed for 5 min at 2000 rpm. Then graphite was added after a 10 min mixing. An additional 2.8 mL of deionized water was used for the slurry. The slurry was cast with a doctor blade on copper foil (Goodfellow, 0.01 mm, 99,9 %), dried under ambient conditions, and cut into discs of 16 mm in diameter (mass loadings: 2–3 mg$_{AM}$ cm^{-1}). Before use electrodes were dried at 120 °C for 12 h under vacuum (10^{-3} mbar).

KFF electrodes. The positive electrode comprised 0.180 g $K_2Fe[Fe(CN)_6]$, 0.030 g of carbon black, and 0.030 g of PVdF (80:10:10 ratio by mass). The materials were weighed in a ball-mill container, and 0.8 mL of *N*-methyl-2-pyrrolidone was added. The container was transferred to a ball-mill mixer (3 balls, ZrO_2, 4 mm), and the slurry was mixed in two 10 min steps. At first carbon black and PVDF with 0.4 mL NMP, in the second step, KFF and 0.4 mL of NMP were added. Subsequently, the slurry was spread onto carbon-coated aluminum foil and dried under ambient conditions. Electrodes with a diameter of 16 mm were cut out and dried at 150 °C for 12 h under vacuum (10^{-3} mbar).

Cells Configurations and Electrochemical Measurements - General. Experiments were performed in either stainless steel (SUS316L) 2032 round button type cells (coin cells) or Swagelok-type cells (Scheme 1). 3e cells were built using the design with modification of the reference materials, specifically K-metal (K-RE), a KFF composite (KFF-RE), or a AgCl-RE, respectively. In brief, the design that was previously reported in ref [12] (Design B) is based on a concentric alignment of a WE-ring electrode and RE in the center. In the original design, the reference material is filled into a cavity in the reference electrode (Scheme 1a). Herein the reference materials were either the alkali metals Li or K (Li-RE and K-RE) or a KFF composite (KFF-RE). The cavity was filled with reference electrode material until it reached the working electrode (WE) level. The setup can also be used for 2e measurements, by using two disc electrodes and leaving the cavity empty. For measurements with AgCl-RE, the RE-component was replaced by the reference cell
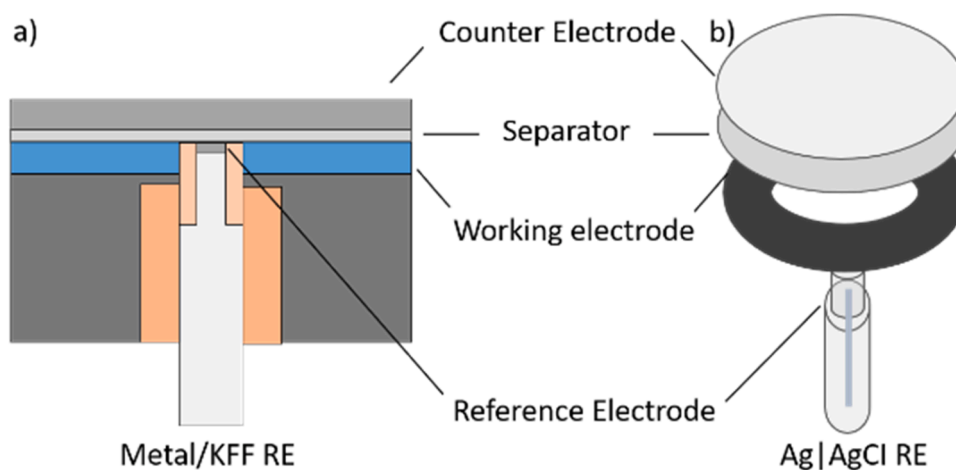
Scheme 1. 3-electrode cell scheme with metal or KFF (a) and AgCl-RE (b) as reference electrodes.

compartment in a glass tube with about the same diameter (as illustrated in Scheme 1b). All 3e measurements with AgCl-RE were performed in an Ar-filled glovebox.

Electrolytes. The base electrolyte formulation comprised of 750 mM KPF_6 in EC:DEC (v/v = 1:1). A second electrolyte formulation was prepared from the base electrolyte by addition of 1 wt.% DTD. In addition, for a control experiment, an electrolyte comprising 500 mM KPF_6 in EC:PC (v/v = 1:1) and 5 vol.% FEC was prepared. Potassium metal electrodes were rolled to thin foils and cut into discs of 16 mm in diameter, prior to cell assembly.

Potentiostat and cell tests. All electrochemical tests were conducted on a Biologic VMP-3 potentiostat. Cycling tests in 3e configurations were performed through control of the cell voltage ($E_{cell} = E_{WE}$-E_{CE}), labeled 'GCPL6 technique' in the Biologic EC-Lab Software (V11.43). In other words, 3e cells cycled with this technique operate as if they were operated in a 2e cell, but in the presence of a RE 'spectator', which is contrary to other 3e cycling protocols that use the potential difference between WE and RE ($E = E_{WE}$-E_{RE}). Therefore, the cut-off limits in this test were defined by E_{cell}. Through the RE, the individual potential changes at the WE and CE could then be recorded vs. the RE potential, but the RE did not take an active role in the cell measurement and control.

AgCl-Reference Electrodes. Ag/AgCl reference electrodes (AgCl-RE) were investigated as inert alternatives to K-metal and KFF composite reference materials in 3e cell setups.

Preparation. Ag wire covered by AgCl was prepared electrochemically. All calibration measurements were performed in a 3e glass cell (5 mL) with a 2 mL working volume. Silver wire (ChemPur Feinchemikalien, 0.25 mm diameter; 99.995 %) was used as a working electrode in an aqueous 100 mM HCI solution with 1 M KCl as supporting electrolyte and a Pt-CE. After 1 cycle of cyclic voltammetry (CV) in [0; 1 V] range at 20 mv s^{-1} the wire was ready to use. The reference electrode (glass tube with Ag|AgCI wire) was filled with a saturated solution of TBACI (99.5 %, Sigma-Aldrich) in the same solvent as that in the working electrode compartment (a mixture of carbonate solvents, such as EC:DEC, v/v = 1:1) to minimize discrepancies in the liquid junction potential between the two electrolyte solutions.

Calibration. The potentials of the respective AgCl-RE were calibrated against the ferrocenium/ferrocene (Fc^+/Fc) redox couple in the EC:DEC solution (10 mM Fc^+/Fc + 100 mM KPF_6 in EC:DEC) between Pt-WE disc electrode (6 mm diameter) and Cu-CE (coil).

Reference potential measurements. The AgCl-RE was employed to determine the electrode potentials of Li- and K-metal foils in the EC:DEC (v/v = 1:1) electrolyte mixtures comprising 0.75 M $LiPF_6$ and 0.75 M KPF_6. For this purpose, a second AgCl-RE was prepared ("AgCl-RE2"). The calibration measurement against Fc^+/Fc is provided in **Figure S4b**.

The two AgCl-REs show a relative shift, which is referred to differences in the AgCl coating on the wire (**Figure S4a**). The potentials in the manuscript are all referred to (*"AgCl-RE1"*). The standard potential of Li and K was determined by cyclic voltammetry in symmetrical Li/Li and K/K 3-electrode cells against the AgCl-RE at a scan rate of 0.05 mV s^{-1} in the potential range from −1.9 to −2.55 V. The redox potential was determined from the zero-current intersect of the anodic and cathodic scan.

Symmetrical cell tests. K/K symmetric cells were assembled both as 2e coin cells and 2e Swagelok-type cells from two 16 mm potassium discs. A single layer of glass fiber separator was positioned between the potassium discs and the separator was soaked with 150 μL of electrolyte. The tests comprised of an initial 6 h OCV step, and constant current cycling at ± 32 μA cm^{-1} in 8 hour steps.

2-electrode (2e) half cell tests. The half-cells were assembled in 2e coin cells and comprised of either a graphite- or KFF-WE and a K-metal counter electrode ('K-CE'). The electrodes were placed between one layer of glass fiber separator, which had been soaked with 150 μL electrolyte, and the cells were then sealed with a coin cell crimper.

Galvanostatic cycling. 2e Coin-Cell tests were conducted under constant-current constant-potential (CC—CP) conditions. Two initial cycles were conducted at C/20. On the following cycles the cycling rate was increased to C/10. (1C = 279 mA g^{-1} (graphite) & 120 mA g^{-1} (KFF)). The lower and upper cut-off voltages were chosen as 0.025–1.2 V vs. K^+/K for graphite and 2.5–4.3 vs. K^+/K for KFF half cells. In the CC step, a time limit of 35 h was set as additional safety measure. In the CV step, the time limit was 30 min and the current limit was equivalent to a current of C/40 in the first two cycles and C/20 in all following cycles.

Self-discharge Test of KFF/K half cells. Several self-discharge tests were conducted in this study. In connection with the KFF-RE studies, a KFF/K-CE electrode with an 750 mM KPF_6 in EC:DEC (v/v = 1:1) electrolyte) was cycled for 1 cycle under CC—CV conditions at a rate of C/20 (with time limitation of 35 h) and a CV phase of 30 min or until the equivalent of a C/40 current cut-off is reached. Then charged in the second sequence to 3.5 V vs. K^+/K, before the cell was put in a 70 h OCV interval. Similar tests were also recorded with KFF/K-CE half cells with the 750 mM KPF_6 in EC:DEC + 1 wt.% DTD and 500 mM KPF_6 in EC:PC (v/v = 1:1) + 5 wt.% FEC electrolyte, respectively. In these tests the cells were first cycled for a full two cycles (cycled between 2.5–4.3 V vs. K^+/K and under CC—CV conditions with a constant current of C/20 and a 30 h time limit; in the CV phase the potential was held for a maximum of 30 min or until the current cut-off of C/40 was reached), and then fully charged to 4.3 V once more. Thereafter, the open-circuit voltage (OCV) was recorded over 100 h. The C-Rate was C/20, with a time limit of 35 h and a CV step of 30 min.

2-electrode (2e) full cell tests. The full cell comprised the graphite

electrode, one glass fiber separators and the KFF electrode were stacked on top of each other (N/P ratio ≈ 1.5). The separators were wetted with 150 μL electrolyte and then sealed with a coin cell crimper. Galvanostatic cycling of graphite/KFF full cells was carried out similar to the half cell tests with a CC—CP cycling protocol. In the initial two cycles, a rate of C/20 was applied, followed by eight cycles at C/10 (C = 120 mAh g^{-1}) between the voltage limits of 2.0 V and 4.15 V. During the CP step, the limiting current was set at C/40 (half the current of the CC step) for the first two cycles, with the cycling rate increased to C/10 from the third cycle onwards. The limiting current in the CP step was increased in accordance with an equivalent of C/20.

3-electrode (3e) Graphite Half Cells with Li-RE and K-RE. For benchmarking tests graphite/K-RE/K-CE and graphite/Li-RE/Li-CE 3e cell configurations were conducted to evaluate drifts and overpotentials of the alkali metal QREs. For both experiments the same graphite electrodes can be used. The ring electrodes were obtained from cutting a 8 mm (in diameter) hole in the center of 16 mm electrode discs. The reference cavity was filled with the respective alkali metal and inserted into the cell setup. The graphite-WE and the reference electrode were covered by two layers of glass fiber separator that were soaked in 450 μL electrolyte (Li: 1 M LiPF$_6$ in EC:DEC (v/v = 1:1), K: 750 mM KPF$_6$ in EC:DEC (v/v = 1:1). A 16 mm Li or K disc electrode was used as counter electrode (Li-CE and K-CE, respectively).

Galvanostatic cycling (Graphite/K-RE/K-CE). The graphite/K half cell was cycled as previously reported with two initial cycles were conducted at C/20, followed by an rate increase to C/10. (1C = 279 mA g^{-1}) within the voltage limits of 0.025–1.2 V vs. K^+/K. In the CC step, a time limit of 35 h was set as additional safety measure. In the CV step, the time limit was 10 min and the current limit was equivalent to a current of C/40 in the first two cycles and C/20 in all following cycles.

Galvanostatic cycling (Graphite/Li-RE/Li-CE). The graphite/Li half cell were cycled for four cycles at C/20 (1C = 372 mA g^{-1}) within the voltage limits of 0.025–1.2 V vs. Li$^+$/Li. In the CV step, the time limit was 10 min and the current limit was equivalent to a current of C/40 in the first two cycles and C/20 in all following cycles.

3-electrode (3e) Graphite Half Cells with KFF-RE. In this experiment the reference cavity was filled with a KFF composite. The rest of the graphite/K half cell configuration remained the same to the 3e experiments with K-RE (see above).

KFF-RE preparation. The KFF-RE needed activation by oxidizing the material to the lower potential plateau at around 3.5 V vs. K^+/K. For the preparation step the KFF-RE was rewired and used as working electrode in a 2e electrode setup against the K-CE in the 3e cell setup, as reported previously in a similar experiment by Holtstiege et al. [30].. In the second cycle the cell was cycled to a potential of 3.7 V in two charging steps, taking into account a larger voltage drop during voltage relaxation of around 200 mV after reaching the targeted end point potential, due to setup-related overpotentials in this phase of the preparation. The stability of the KFF-RE against K-CE in this configuration was studied over 10 h at OCV.

Galvanostatic cycling (Graphite-WE/KFF-RE/K-CE). The graphite/K half cell with KFF-RE was cycled for three cycles at C/20 (1C = 279 mA g^{-1}) within the voltage limits of −3.42 V to −2.2 V vs. KFF-RE. In the CV step, the time limit was 30 min and the current limit was equivalent to a current of C/40 in the first two cycles and C/20 in all following cycles.

3-electrode (3e) cell setups with AgCl-RE. For this setup, the reference electrode pin in the Swagelok-type cell was replaced by the AgCl-RE capillary, which fit in diameter. In addition, the capillary was fixed in place and sealed around the reference electrode inset.

3e-Graphite/K, 3e-Graphite/Li and 3e-KFF/K Half cells. Graphite-WE or KFF-WE ring-electrodes were prepared from 16 mm electrode discs by cutting a hole in the center of the disc with 8 mm in diameter. The ring-WEs covered by two Whatman GF/B separators that were soaked with 450 μL of electrolyte. Graphite half cells were assembled both with Li-CE and K-CE. In addition, the CE was covered by a layer of Celgard separator in half cell measurements.

Cyclic Voltammetry (CV) on KFF Electrodes. 3e KFF/AgCl-RE/K-CE configurations were studied by CV in a voltage range from 0.4 V to 1.8 V vs. AgCl-RE. The scan rate was 1.5 mV min^{-1} (25 μV s^{-1}).

Galvanostatic cycling. The cut-off voltage in graphite/K-CE half cells was 0.025 V and 1.3 V vs. K^+/K. The same limits were applied vs. Li-RE in the respective half cell tests with a Li-based electrolyte. The voltage limits for KFF/K-CE half cells were 2.5 V and 4.3 V vs. K^+/K. To minimize influences from polarization effects, three-electrode half cells with AgCl-RE and Li-RE were measured at a constant current rate of C/20 In the CV step, the time limit was 10 min and the current limit was equivalent to a current of C/40 in the first two cycles and C/20 in all following cycles (active material masses (without DTD/with DTD): KFF 5 mg / 4.4 mg; graphite 2.85 mg / 2.85 mg).

Full cells. KFF/graphite full cell assemblies comprised of a graphite ring-electrodes against a KFF disc and two Whatman glass fiber separators soaked in 450 μL of electrolyte). The electrode masses were balanced around a N/P ratio of 0.62–0.72 to compensate for the significant losses of charge carriers on the first cycle. The active material masses for the 3-electrode measurements on the DTD-free and DTD-containing electrolyte (Fig. 6) were 4.5 mg (graphite) and 16.4 mg (KFF) and 5.0 mg (graphite) and 15.8 mg (KFF), respectively. N/P ratios were based on the practical charge capacity of KFF (110 mAh g^{-1}) and discharge capacity of graphite (250 mAh g^{-1})[7] in half cells, following the data presented in **Figure S2a & S2b**.

Galvanostatic Cycling. The cycling parameters were identical to those employed in two-electrode cells, i.e. two initial cycles were conducted at C/20, before the rate was increased to C/10 within the voltage limits were 2 V and 4.25 V. In the CV step, the time limit was 10 min and the current limit was equivalent to a current of C/40 in the first two cycles and C/20 in all following cycles.

3. Results and discussion

3.1. Reference electrodes for KIBs

In this section three different reference electrode systems are discussed: a) K-metal as reference ('K-RE') and quasi-reference ('QRE') electrode, b) a partly charged K$_2$Fe[Fe(CN)$_6$] (KFF) and c) an AgCl-RE in a separate reference cell compartment. For the following tests, different cell configurations are employed to outline the pros and cons between the three REs. Besides the K-K symmetric cells, half cell and full cell configurations were built from common electrode materials, namely graphite as the negative electrode and KFF as the positive electrode. The standard electrolyte formulation in this section was a mixture comprising 0.75 mM KPF$_6$ in EC:DEC (v/v = 1:1). Unless stated differently, experiments were performed in the cell design provided by Bünzli et al. [12] (Scheme 1).

Potassium metal reference or quasi-reference (K-RE/K-QRE). In a first step, stripping/plating experiments in a symmetric 2e setup were performed to quantify the electrode polarization and potential drift over time, which is a measure of the reactivity and stability of the K-metal electrode in the respective electrolyte[8,28]. The potential profile over the first 160 h is shown in Fig. 1a. During the open-circuit voltage (OCV) phase (the initial 5 h), the cell voltage was slightly offset from 0 V (−2 mV). At a constant current of 32 μA cm^{-2} the overpotential remained relatively stable and symmetric around a potential of ±41 mV and a time-dependent potential drift of 5 mV over a period of 155 h. For short-term experiments (<200 h), this level of potential drift appears acceptable. Interestingly, the Swagelok-type cell (Scheme 1) exhibits a lower degree of polarization than that observed in corresponding coin cells experiments (**Figure S1**), which could be due to different stack pressures.

However, it has been shown that the voltage profile of potassium, acting as a QRE in 2e configurations, is significantly affected by both the electrolyte composition and the applied current density [3,8,13]. Furthermore, in the aforementioned reports [3,13] a notable offset of

a) K/K symmetrical cell (2-electrode)
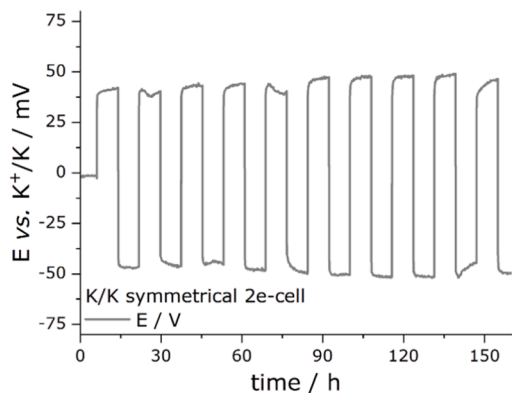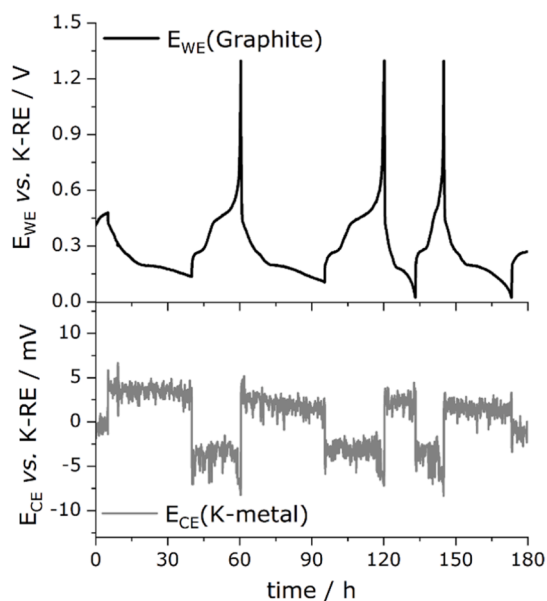

b) Graphite/K-RE/K-CE 3-electrode cell

Fig. 1. a) Voltage profile of K-WE vs. K-CE (i.e. vs. K^+/K) in a 2-electrode symmetric cell setup (current density 32 μA cm^{-2}), b) 3-electrode measurements with K-RE. The top panel shows the potential profile of graphite vs. K-RE (the first two cycles were conducted at C/20 with an additional 35 h time limitation, followed by cycling sequences conducted at C/10), the bottom panel that of K-CE vs. K-RE. The experiments were conducted in an electrolyte comprising 0.75 mM KPF$_6$ in EC:DEC.

the initial OCV was observed that was related to impurities in the K-metal, especially at the electrode surface. This highlights a strong dependence of K-RE on the grade of the purchased potassium and its preparation into electrodes [20,31,32].

For experiments in 3e setups the cell design reported by Bünzli et al. [12]. was used with an K-metal reference (K-RE), K-metal counter electrode (K-CE) and graphite as working electrode (Gr-WE). The voltage profiles for Gr-WE vs. K-RE are shown in the top panel of Fig. 1b. As in 2e coin-cell setup (**Figure S2a**) the profiles show the (de)intercalation process of K-ions at the graphite electrode with multiple intercalation stages.

In contrast to graphite lithiation, potassium insertion lacks clear potential plateaus and instead has two sloping sections. The first section shows a steeper potential slope, ranging from 500 mV to 250 mV, which includes disorderly stacked graphite intercalation compounds (GIC) stages ranging from KC$_{96}$ to KC$_{16}$. The last step, the conversion of KC$_{16}$ to

KC$_8$ is a plateau-like section in the potential range below 250 mV vs. $K^+/$K [33,34]. As previously reported by our group[4] the first two formation cycles are performed with a time limit of 35 h per cycling sequence. Within this time interval the electrodes did not reach the lower cut-off limit of 25 mV vs. K-RE (3e) and vs. K-QRE (2e) during intercalation, which is clearly seen from the potential profiles in Fig. 1b (top). The deintercalation reaction proceeds *via* a two-step profile with a sharp increase in potential at the end of discharge until the upper cut-off limit of 1.2 V is reached. As previously reported, the concentration of electrolyte degradation products in presence of K-metal is substantial [1,2] and the thick surface layers found in previous studies by X-ray photoelectron spectroscopy (XPS)[4] indicate overall a high degree of irreversible reactions that prolong the intercalation process on the first cycles [7]. Furthermore, in the 3rd cycle, i.e. after increasing the C-rate from C/20 to C/10, the cycling sequence was overall shorter, but reached the lower end point potential. In the 3e setup it is further possible to follow the K-CE potential profile, as shown in the bottom panel in Fig. 1b. The polarization of K-CE vs. K-RE is lower than in the K/K symmetric cell experiment in Fig. 1a and lies between ±4 mV with a noise level of the K-CE potential of less than ±1.5 mV.

Issues with partly charged KFF as reference electrode (KFF-RE). Partially charged cathodes have been used successfully as REs in LIBs, for example partially charged LiFePO$_4$ [35] or Li$_4$Ti$_5$O$_{12}$ [19] for Li half cells. A similar approach is examined herein, by using partly charged KFF as reference in a 3e setup with a Gr-WE and K-CE.

3e-experiments with KFF-RE. For this experiment the reference cell cavity of the Swagelok-type cell introduced in Scheme 1 was loaded with a KFF electrode formulation. The 3e cell further comprised of a Gr-WE and K-CE. Before the actual experiment, the KFF-RE was conditioned in this setup by connecting the cell to a 2e configuration against the K-CE, similar to a previous study by Holtstiege et al. [30].. For activating the material, the KFF-RE was first cycled for one full cycle before it was oxidized in the subsequent sequence to a target potential of 3.70 V vs. $K^+/$K. (Fig. 2a). The voltage profile of the KFF-RE/K-CE setup shows the characteristic 2-step process with a sloping section in the high potential region until the cut-off is reached at 4.3 V, in accordance with previous results[10,29]. Compared to coated electrodes the overpotential in this setup was about 200–300 mV higher, which is also indicated by the IR drop when the cell entered the OCV phase at the end of the experiment, resulting in a voltage relaxation onto the first voltage plateau at around 3.40 V vs. $K^+/$K. The OCV remained constant for a duration of 10 h (Fig. 2a, green area), after which the cell was reconnected to the 3e configuration.

The Gr-WE was cycled with similar settings as in Fig. 1b (**top**) but to a lower cut-off limit of −3.375 V vs. KFF-RE (the OCV potential in the 2e configuration). Fig. 2b shows the cell voltage (Gr-WE vs. K-CE) in the top, E(Gr-WE) vs. KFF-RE in the middle and E(K-CE) vs. KFF-RE in the bottom panel, respectively. The voltage profile is at first comparable to the ones shown in Fig. 1b **(top)** but with a several-hour-long plateau at 0 V, which likely indicates K-metal plating. When the individual electrode potentials with respect to KFF-RE are examined, it is observed that both profiles display a strong potential drift of 400 mV after 150 h. As will be demonstrated below, this effect is attributed to a drift in the KFF-RE potential, specifically from originally 3.4 V to ca. 3.0 V. During the first cycling sequence, i.e. K-intercalation into graphite, the Gr-WE potential decreased, while at the same time the KFF-RE potential drifted in the same direction, rendering the set cut-off limit unattainable. Ultimately, a constant K-plating potential is reached for the remaining duration of the sequence until the time limitation stopped the process (i. e., Gr-WE and K-CE potentials drift with similar slope, to the drift of KFF-RE).

Self-discharge of KFF electrodes. For the further investigation of the significant potential drift of KFF in the above 3e setup, experiments in 2e KFF/K-CE cells were conducted (Fig. 2c). In the standard EC:DEC electrolyte mixture, an additional charge plateau at a potential of approximately 3.8 V vs. K-CE (Fig. 2c) is seen. From previous experiments in
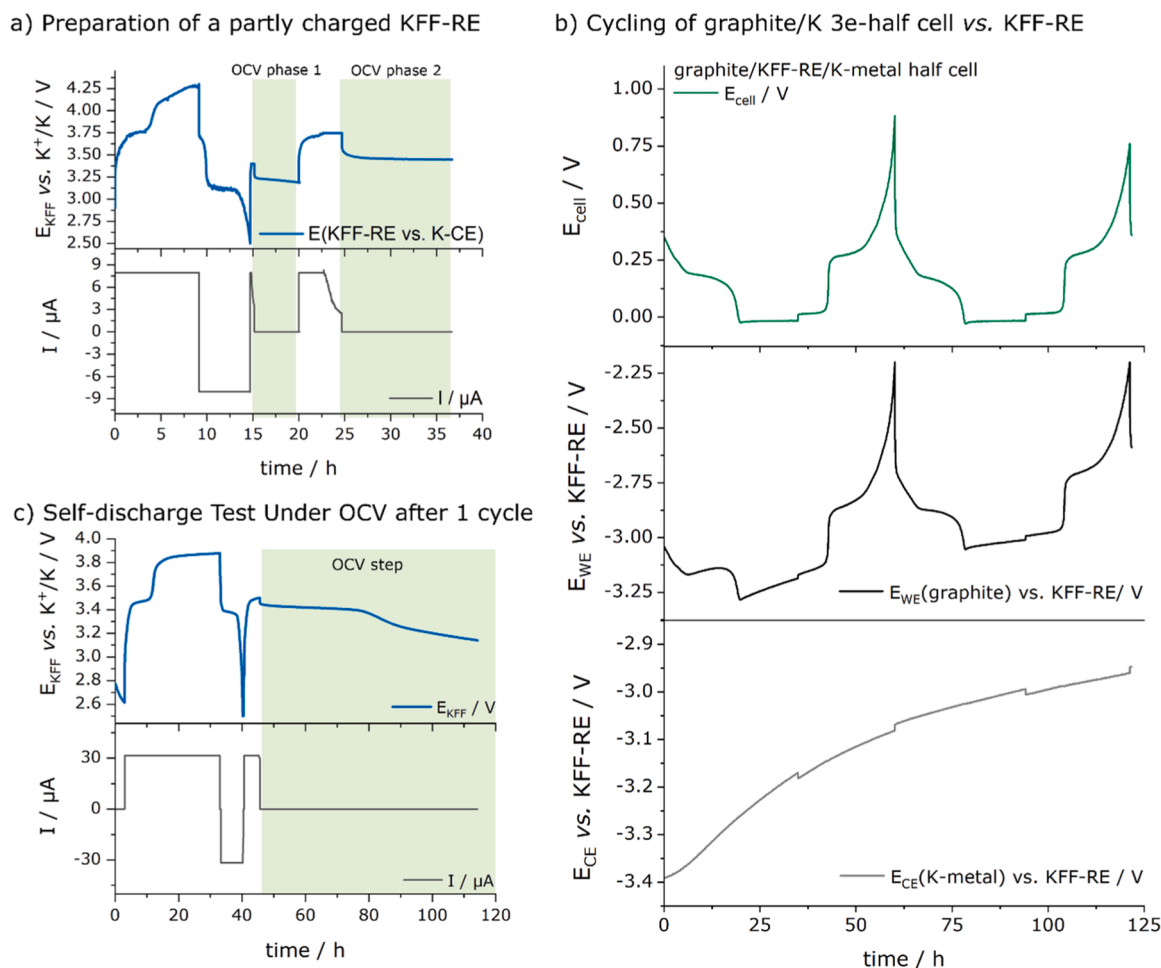
Fig. 2. a) KFF-RE preparation in a 3e Gr-WE/K-CE/KFF-RE setup. The KFF-RE electrode was cycled in a (rewired) 2e configuration (KFF vs. K-CE) for 1 cycle and then charged to the lower voltage plateau in two constant potential-OCV steps in the next sequence (marked in green). b) 3-electrode measurements with KFF-RE. The top panel shows the cell voltage of graphite vs. K-CE, the middle panel displays the potential transient of graphite vs. KFF-RE and in the bottom panel the potential profile of K-CE vs. KFF-RE is shown. The cell was cycled under a constant current (C/20,) with 35 h time limit. c) Self-discharge test of KFF in a 2-electrode setup against K-CE: The cell was cycled for 1 cycle at C/20 (i.e. 14 mA g^{-1} with 30 h time limit), then charged to 3.5 V on the next sequence followed by a OCV interval (marked in green). Electrolyte: 0.75 mol l^{-1} KPF$_6$ in EC:DEC.

other electrolytes and from literature, this potential is below the second redox reaction of KFF. Hence, a significant fraction of the upper potential region is likely ascribed to irreversible reactions during the oxidation step on the first cycle. Interestingly, it was the cell setup that seemed to determine whether or not the cell reached the upper cut-off on the first cycle. In certain instances, this side reaction is so pronounced that the cell is unable to achieve a complete charge initially, as evidenced by an extended potential plateau of 20 h at 3.8 V (Fig. 2c). With the time limit of 40 h in place, the second plateau typically appears after two or three cycles, indicating formation of a sufficiently protecting surface layer.

When the cycling protocol of the KFF-RE activation is applied on such a cell and the OCV period is prolonged, a voltage profile such as the one shown in Fig. 2c (green area; OCV phase) is obtained. The current was stopped after the cell reached 3.5 V on the second cycle. After the initial IR drop to 3.4 V, the voltage decreased slightly by 40 mV, until a marked voltage drop after ca. 40 h marked an accelerated voltage decrease that approached 3.2 V after another 30 h at OCV. Such intermittent OCV sequences during cell tests are rather uncommon, which is why such effects can easily be overlooked. The delay between onset of OCV and accelerated voltage drop is an indication that a diffusion process is involved, which resembles the behaviour in Li-S batteries[36,37] for example. We suspect that the SEI components in the surface layer of K-CE dissolve over time, making the K-metal surface more accessible to

electrolyte components and resulting in the formation of soluble degradation products. For Na-ion batteries, the tendency of SEI components to be more soluble was demonstrated previously by Mogensen et al. [38]. and Mo et al. [39]. using intermittent OCV sequences in their cell cycling. In agreement with our results, Lee and Tang observed in a previous study potential drifts of KNi[Fe(CN)$_6$] with a steep potential step after 20h[22]. Similarly, severe crosstalk was reported in K-ion setups by several groups [3,4,28] as early as the first OCV phase after cell assembly. As recently shown by our group, the formation of soluble degradation products from EC and DEC is strongly accelerated in presence of K-metal and leads to formation of diethyl 2,5-dioxahexanedioate (DEDD)[1,28], which Hosaka et al. [3]. could clearly correlate to high degrees of irreversible reactions at the positive electrode (in 2e half cell setups) due to crosstalk. The authors suggested the use of the electrolyte additive 1,3,2-dioxathiolane 2,2-dioxide (DTD) or fluoroethylene carbonate (FEC) in order to passivate the K-metal surface and suppress the DEDD formation, which is in fact a viable approach, as demonstrated in the corresponding self-discharge tests in these electrolytes in **Figure S3a & S3b**.

While practical considerations of suitable electrolytes often suffice for material testing, as long as the formulation provides a common basis for comparison, it is essential for robust REs to be applicable in a broad range of electrolyte formulations and compositions. In addition, if only specific formulations would be used, like PC-containing solvents or the

DTD-additive, compatibility problems with electrodes may arise, as will be demonstrated below. In the case of KFF-RE, the use of the RE is thus restricted to a limited number of formulations and therefore impractical.

Self-discharge induced by K-RE in full cell configurations. Our findings would suggest that any introduction of metallic potassium inevitably leads to formation of DEDD that induces the observed self-discharge at the KFF electrode. Therefore, the experiments were expanded to full cells with a metallic reference, K-RE. A comparison of voltage profiles obtained from a Gr/K-RE/KFF 3e cell (red) and KFF/K-CE 2e cell (blue) is provided in Fig. 3a. Furthermore, the cell voltages of both a 2e KFF/ graphite (i.e. a K-metal-free cell) and the 3e KFF/K-RE/graphite full cells are also shown for comparison, in Fig. 3b and 3c, respectively.

Firstly, in Fig. 3a, the potential profiles between the 2e and 3e cells are slightly shifted against each other on the voltage axis, as a result of the polarized K-QRE in the 2e half cell setup. More importantly, both cells display a 2-step voltage profile in the voltage region above 3.75 V where only one would be expected (see also Fig. 5). In contrast, when the potential profile of the KFF electrode (vs. K-RE) is compared to the K-metal-free 2e full cell in Fig. 3b (blue) the second voltage step above 3.7 V disappeared (note that in the profile of the 2e cell only the cell voltage between graphite and KFF is shown). The 2e cell reaches the upper voltage cut-off limit of 4.25 V after ca. 20 h, whereas the potential of the 3e cell (Fig. 3c, red) with K-RE increased notably slower and only to a maximum potential of 4.10 V on the first cycle. While the 3e cell reaches the upper cut-off on the 2nd cycle as well, the second high-potential feature from irreversible reactions can still be observed clearly.
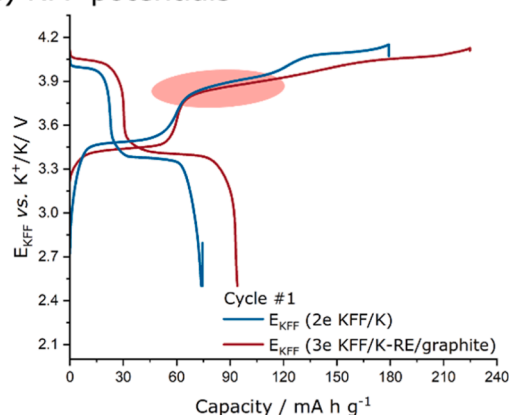
Comparing the profiles in Fig. 3a and 3b between charge and discharge, it can be illustrated clearly that the 3e cell, as well as the 2e KFF/K-CE half cell suffer considerably more from parasitic processes than the 2e KFF/Gr full cell without any K-metal. This is also manifested in the 3e cell by a low Coulombic efficiency (C.E.) of 43 % on the first and 68 % on the second cycle. Although, the 2e KFF/Gr full cell displays considerable irreversible losses, leading to a rapid disappearance of the lower voltage step, its first cycle C.E. was 12 % higher. Interestingly, the first cycle discharge capacities were higher for the 3e cell (95 mA h g^{-1} *vs.* 76 mA h g^{-1}), despite lower C.E. and similar balancing. Although the origin of this effect is unclear, it might be an effect of the additional K-source from K-RE.

In summary, even small amounts of K-metal, e.g. in form of a K-RE, can be sufficient to induce additional electrolyte degradation processes in full cell configurations and thus K-RE electrodes are a problem in these setups.
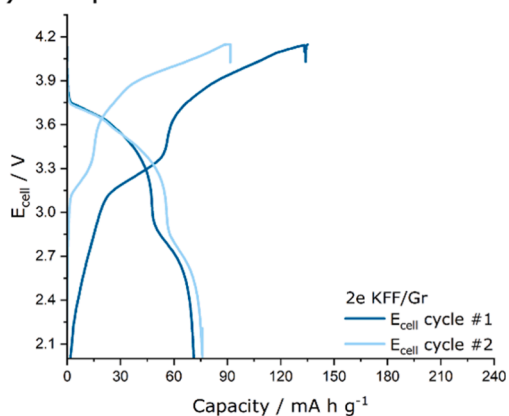
Ag/AgCl reference electrodes (3-electrode setup). For electrochemical experiments in non-aqueous systems Ag wire (i.e. Ag/Ag_2O) and Ag/AgCl reference electrodes could be used [20,24]. Because of the vast variety of different solvents used for battery electrolytes, it should be possible to transfer the electrode into different media to avoid the influence of junction potentials. The reference potential can be checked across different electrolyte formulations by use of an internal reference redox couple, herein Fc^+/Fc.

AgCl-RE in a 3e battery cell setup. The original cell developed by Bünzli et al. [12] was designed for metallic RE, but the construction allows to replace the RE inset with a standard AgCl-RE electrode in a glass capillary with membrane (Scheme 1), which can be used in any electrochemical measurement, allowing it to be used in coin cell-like experiments and to validate RE potentials vs. the Fc^+/Fc redox couple in the electrolyte of choice. The AgCl-RE and the revised cell setup was first evaluated in a comparison of the potential transients of 3-electrode Li/graphite cells against either a Li-RE or AgCl-RE. The Li-systems seemed a better choice for validation of the two Res, for the flat and characteristic potential plateaus during the Li (de)intercalation. The respective potential profiles of the Gr-WE (top) and Li-CE (middle) half cell reactions are plotted for either Li-RE or AgCl-RE in Fig. 4a. Both cells show the characteristic potential transient of the Li-intercalation into graphite and yield similar capacities (353 and 362 mA h g^{-1} respectively). More importantly, no differences or drifts were observed for the
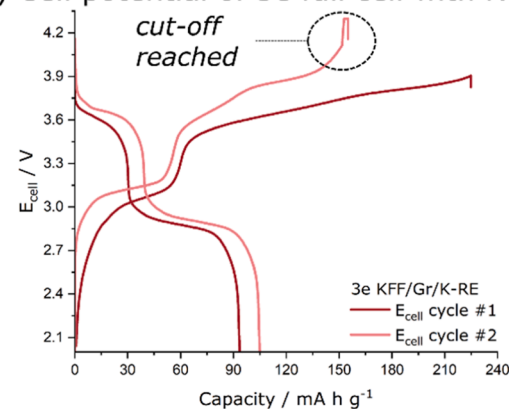

Fig. 3. Comparisons of a) KFF potential on the first cycle in a KFF/K-RE/graphite 3e full cell and 2e KFF/K half cell. To demonstrate further the influence of K-metal, even in small quantities the cell potentials of full cells on the 1st and 2nd cycle are presented in b) for a 2e KFF/Gr full cell (i.e. without K-metal in the cell) and in c) a corresponding 3e KFF/graphite full cell with a K-RE. The electrolyte for all experiments was 750 mM KPF_6 in EC:DEC (v/v = 1:1). The cells were cycled at a C-rate of C/20.

potential profiles of the Gr-WEs.

Interestingly, the Li-CE showed different polarization behavior depending on the type of reference electrode. Against Li-RE, the Li-CE declined within the 5 h OCV phase from 3 mV to 0 mV. During the cycling process, the Li-CE polarization reached 11 mV initially and remained at around 8 ± 2 mV on following cycles. In contrast, against AgCl-RE, the initial OCV drift was more significant, reaching 17 mV (from −2.281 to −2.298 V) for Li-CE at the end of the OCV phase. The
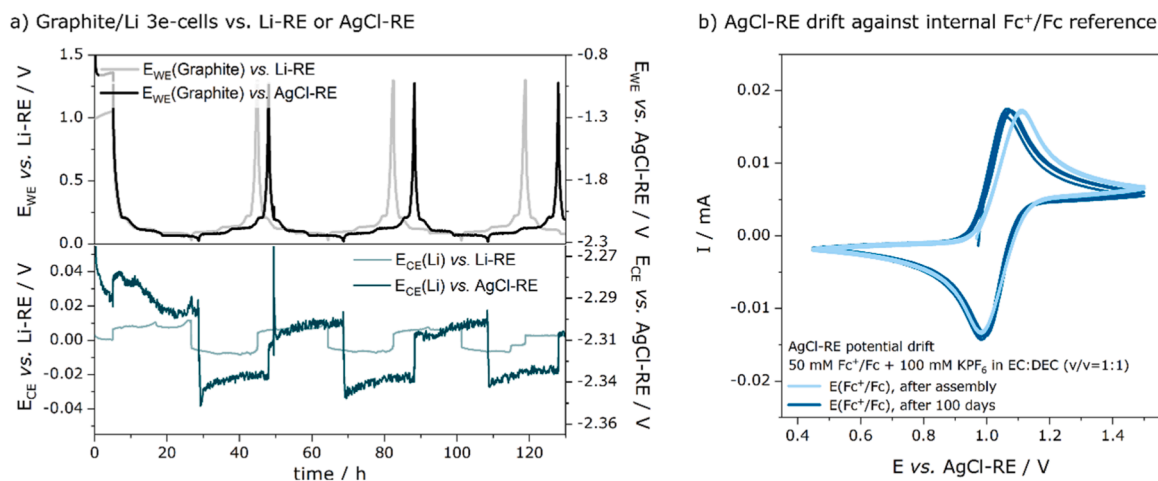
a) Graphite/Li 3e-cells vs. Li-RE or AgCl-RE

b) AgCl-RE drift against internal Fc⁺/Fc reference

Fig. 4. a) Potential profiles from Graphite/Li 3e-cells vs. Li or AgCl-RE in 1 M LiPF$_6$ in EC:DEC (v/v = 1:1) that were cycled at a rate of C/20. and b) aging and potential drift of AgCl-RE after assembly and after 100 days by comparison of cyclic voltammograms (scan rate 20 mV s^{-1}) in 100 mM KPF$_6$ and 10 mM Fc⁺/Fc in EC: DEC, v/v = 1:1 electrolyte (against Pt and Cu electrodes).

start of the cycling sequence caused a positive potential jump at the Li-CE to around 30 mV, which declined within the first charge sequence back to around 15 mV. While the electrode potentials during the charging sequences were similar in the Li-RE and AgCl-RE cells, a higher polarization of the Li-CE vs. AgCl-RE was observed in the discharge sequences, with values reaching up to 30 mV.

Stability of AgCl-RE in carbonate solvents. Aging of the AgCl-RE over 100 days was first studied in a 3e setup with a Cu-CE (coil), a Pt-disc WE and 2 mL electrolyte solution (100 mM KPF$_6$ and 10 mM Fc⁺/Fc in EC: DEC, v/v = 1:1). As seen from the CV curves in Fig. 4b there was no change observed in the cathodic half-wave potentials of the cathodic sweep. The anodic half-wave potential decreased by 22 mV. The observed drift of the AgCl-RE is likely attributed to minor degrees of electrolyte evaporation over time and possible changes at the Ag-wire surface. For instance, the formation of the soluble [AgCl$_2$]⁻ complex can occur in organic solvents [40].

AgCl-RE Reference Potentials. The use of the AgCl-RE in the potassium cell allows for the estimation of the K^+/K electrode potential in EC:DEC-based battery electrolytes. The standard electrode potential of potassium in PC has been calculated by Marcus [41] using standard Gibbs solvation energies and by Matsuura [42] against SCE (saturated calomel electrode). The resulting value is approximately −0.09 V vs. Li⁺/Li in both works. However, there is limited experimental data on the electrode potential of alkali metals in battery electrolyte solvents or solvent mixtures, like EC:DEC. Therefore, the use of AgCl-RE presents an opportunity to experimentally determine the potentials in these solvent mixtures. The alkali metal potentials of lithium and potassium were determined by conducting cyclic voltammetry stripping/plating experiments. The standard electrode potentials (E$_0$) were then calculated by

means of the Nernst equation using the crossover potential of the anodic and cathodic sweep in the zero current region (Table 1, **Figure S4a**). For K-metal in the EC:DEC-based electrolyte, E$_0$(K^+/K) was −0.19 V vs. Li⁺/Li, which is close to previously reported literature data by the Komaba group[43]. The authors observed potassium plating/stripping at an electrode potential of −0.15 V vs. Li⁺/Li in 0.5 M KPF$_6$ EC:DEC.

3.2. The DTD additive studied in a AgCl-RE based 3e setup

The use of 3e setups with AgCl-RE enables a look at electrode processes at the WE and CE without risking adverse interferences of degradation products. In this section, the use of the AgCl-RE setup is validated in a comparison between the EC:DEC-based standard electrolyte with and without the electrolyte additive DTD in different cell setups. According to the recent work by Hosaka et al. [3], DTD is one of the most effective additives to mitigate electrolyte decomposition at the K-metal electrodes and thus suppresses DEDD[44]. However, as reported by the authors, DTD was not well compatible with the graphite electrode. In the 3e cell experiments presented below, the voltage cell measurement and control are done between WE and CE (i.e. cycled like a 2e setup) and AgCl-RE acts merely as a 'spectator' to follow the potential at each electrode individually.

Cyclic voltammetry on KFF/AgCl-RE/K cell. The reaction potentials of the KFF electrode in both electrolytes were first examined in CV experiments (Fig. 5). KFF has two major peaks on the cathodic scan are expected, i.e. the conversion of K$_2$Fe[Fe(CN)$_6$] to KFe[Fe(CN)$_6$] at around 0.95 V vs. AgCl-RE (0.93 V for 0 wt% and 0.96 V for 1 wt% DTD), and the second conversion of KFe[Fe(CN)$_6$] to Fe[Fe(CN)$_6$] at around 1.58 V vs. AgCl-RE. However, in the DTD-free electrolyte (red curve) a third process is observed. Starting from around 1.2 V, two peaks with similar peak current appear in the voltammogram at 1.48 V and 1.58 V vs. AgCl-RE. This is in accordance with the 2-step voltage profile at potentials above 3.8 V vs. K^+/K. Judging from the backward scan, the peak centered at 1.48 V vs. AgCl-RE has no corresponding redox species, which suggests that this peak originates from irreversible reactions and strongly overlaps with the second oxidation step of KFF. As it is located below the second redox potential of KFF, the cathode material cannot be fully charged in the half cell (i.e. in the presence of K-metal). In contrast, the cell with DTD-containing electrolyte (blue) displayed notably smaller peak currents in the potential region above 1.2 V on the first scan for this irreversible reaction (located at 1.42 V). Its peak current decreases notably on the second scan. In presence of DTD the redox processes at 0.80 V in the additive-free electrolyte (anodic sweep) shifts by +40 mV, while above the electrolyte degradation potential, both the

Table 1
The electrode potentials determined from the anodic/cathodic crossover potential in a cyclic voltammetry measurement for both K- and Li-metal electrodes in EC:DEC-based electrolytes against a AgCl-RE with EC:DEC-based reference solution. The resulting potentials are reported against the AgCl-RE ("AgCl-RE1") and the Fc⁺/Fc redox couple (Fig. 4b).

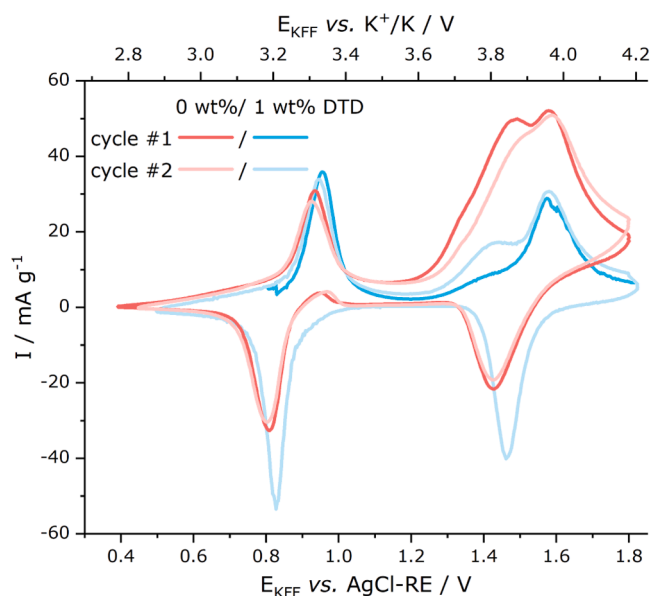| electrode potential	reference electrode	solvent in *reference* compartment	E / V vs.	
			AgCl-RE	Fc⁺/Fc
Li⁺/Li	AgCl-RE	EC:DEC (v/v = 1:1)	−2.36	−3.40
K^+/K	AgCl-RE	EC:DEC (v/v = 1:1)	−2.55	−3.59

Fig. 5. Cyclic voltammogram (scan rate: 25 μV s^{-1}) of a KFF/K 3e cell in EC: DEC 750 mM KPF$_6$ with (blue) and without (red) DTD.

peak position and the potential difference of the redox peaks in the electrolyte without DTD increase with respect to the electrolyte with 1 wt% DTD. Comparison of peak area-ratios between anodic and cathodic sweep in the voltage region above 1.2 V, yields a ratio of around 8 for the additive-free electrolyte. This highlights the large degree of irreversible processes at the electrode in absence of the DTD additive. The latter exhibits a peak area-ratio of only 1.6.
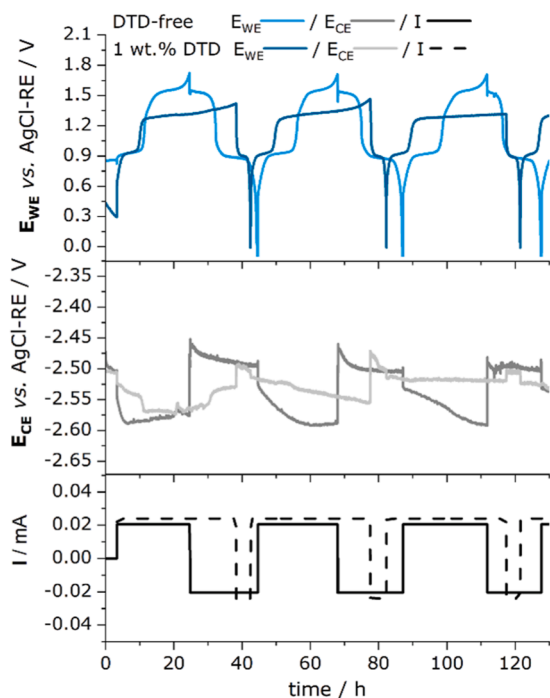
Half cell experiments with AgCl-RE. Both KFF and graphite were

then studied in 3-electrode galvanostatic cycling experiments. The potential profiles of WE and CE vs. AgCl-RE for the four cells are shown in Fig. 6.

Working electrode potentials. The results provided in Fig. 6a (top panel) for the KFF/AgCl-RE/K half cell are largely in accordance with the experiments by Hosaka et al. [3] namely for KFF/K half cells a long electrolyte decomposition plateau of the KFF-WE potential is observed (as suggested by the CV experiments and Fig. 5 above) and the upper cut-off limit is not reached before the time limit of the experiment. In contrast, in the electrolyte with DTD additive, the characteristic 2-step reaction of KFF is observed and the upper cut-off limit is reached at the end of oxidation. For the graphite/AgCl-RE/K configuration for Fig. 6b (top panel), it is worth noting that graphite in the DTD-containing electrolyte shows larger polarization, a fast potential drop at the beginning of the intercalation process and a sloping profile that is absent of the typical intercalation features described above (Fig. 1b), which is also in agreement with the previous work of Hosaka et al. [3]. Because of the high polarization and rapid potential drop, the electrode cannot reach a fully charged state before reaching the lower cut-off limit. The voltage noise in the potential profile of the electrode in the additive-free electrolyte could not be removed but disappeared after the first cycling sequence (thus excluding loose contacts as possible cause), and was observed in other tests (e.g. **Fig. S5**) with additive-free EC:DEC-based electrolytes with K-metal electrodes as well.

The K-CE potentials. Using the AgCl-RE, analysis of the K-CE potentials is possible in the four samples, given in middle panels of Fig. 6a and 6b, that so far have not been analyzed in literature with exception of symmetric cell tests [8,13,45]. The results suggest that the potential profiles of K-metal electrodes are profoundly different from symmetric cells and thus worth discussing. In both the KFF/K and Gr/K configurations K-CE in the DTD-containing electrolyte shows generally larger overpotentials than in the corresponding additive-free case. Previously reported symmetric cell data [3,46] suggested lower overpotentials for

a) KFF/AgCl-RE/K-CE 3e-cells

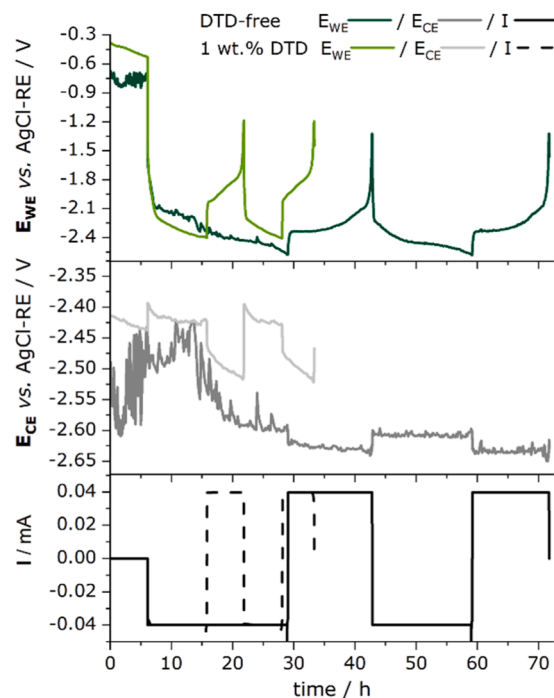
b) Graphite/AgCl-RE/K-CE 3e-cells

Fig. 6. 3e half cell experiments against a AgCl-RE in EC:DEC-based 750 mM KPF$_6$ electrolytes with and without DTD (1 wt.%) as electrolyte additive in a) KFF/AgCl-RE/K-CE half cells and b) graphite/AgCl-RE/K-CE half cells. The top panels show the working electrode (KFF or graphite) potential, E$_{WE}$ vs. AgCl-RE; the middle panel display the K-CE potentials, E$_{CE}$ vs. AgCl-RE. In the bottom panel the applied current, I, is shown. The applied current corresponded to galvanostatic cycling rates of C/20.

DTD-containing electrolytes. Herein, the opposite seems to be the case, both in the 3e cells and the symmetric cell tests above. This might be related to the history and surface conditions of the potassium electrode [13,31,46]. Unlike the symmetric cell data in Fig. 1, notable potential drifts are observed in the potential transient and, in case of additive-free electrolytes, also sudden jumps and fluctuations over tens of mV. This behavior is well reported in literature and is generally ascribed to a significant degree of chemical processes at the potassium metal surface upon contact with the electrolyte. Potential differences of several hundred mV in symmetrical cells after assembly have been reported[13,47]. The K-CE potentials in the first cycling sequence showed tremendous differences, especially in the Gr/K half cell (Fig. 6b) cycled without the DTD additive that experienced potential fluctuations of up to 160 mV in the first hours of the experiment. The potential spikes in Fig. 6b are also seen in the profile of the WE and typically disappeared after the first cycling sequence. In agreement with earlier studies by Hosaka et al. [13]., the potassium metal potential is more stable after the first plating/stripping cycle. Given the stability of AgCl-RE demonstrated both in the Gr/Li setup and in the aging test over the first 100 days (Fig. 4) strong fluctuations originating from the RE are not expected. However, beyond the aforementioned reactivity of EC and DEC at the K-metal surface, the pressure of the RE capillary onto the cell separators in our 3e setup is susceptible to changes (e.g. glovebox vibrations and atmospheric pressure changes inside the box).

An interesting aspect of the potential profiles of the Gr/K half cells are the relative reaction potentials of K-CE in dependence of the electrolyte formulation. In presence of the electrolyte additive DTD, the average reaction potential shifts by nearly +200 mV with respect to the K-CE potential in the additive-free electrolyte. The potential shift leads to premature approach of the lower cut-off limit and thus termination of the cycling sequence, which is clearly seen by comparison of Gr-WE potentials in the top panel. With respect to the AgCl-RE, it is the K-CE potential moving upwards rather than the Gr-WE potential dropping too fast that triggers the lower cut-off limit in a 2e cell. As a result, the graphite electrode cannot reach its fully charged state. Shifts in electrode potentials, as opposed to higher overpotentials around the 0 V potential of potassium, have so far only been reported in the context of weakly solvating or concentrated electrolytes[48,49], while electrolyte or additive degradation typically lead to different SEI properties and hence to changes in overpotentials and the kinetic stability (rather than thermodynamic changes)[2,3,20]. Hence, it is interesting that the potential shift only occurs in one current direction (oxidative current), because in the KFF/K cells, both K-CE potentials show a similar OCV potential in the small resting step between cycles of −2.51 V. This would suggest that under an initial anodic current (as in the case of KFF/K), where K-ions plated onto K-CE the surface chemistry of K-metal remains similar, while under cathodic current, where K-ions are removed from K-CE, the redox potential of K-CE shifts to higher potential as a result of a significant change in surface chemistry. Moreover, it is worth highlighting that the potential profiles of K-CE do not reflect the profiles observed in symmetrical cell tests (Fig. 1 **and S1**), neither with nor without DTD additive.

DTD in 3e full cell setups. The role of DTD at the potassium CE raises the question of how suitable DTD is in absence of a reactive metallic CE? For this test a 3e full cell setup was chosen with a graphite negative electrode, a KFF positive electrode and the AgCl-RE in order to avoid the use of K-metal for the reasons stated above. The potential profiles of the first cycles is shown in Fig. 7, for the KFF-WE, Gr-CE and the cell potential (E_{cell}). In this experiment a cathode areal capacity excess corresponding to a P/N ratio of 1.5 was used, in order to compensate for initial losses. Furthermore, the ratio permits the observation of the impact of the additive on the graphite behavior in a systematic manner. Additionally, it can be observed that AgCl-RE has no significant impact on the electrodes cycling curve. It is important to note that the chosen P/N ratio may not be optimal, and the impact of the additive may vary depending on the P/N ratio. KFF-WE potential curves in cells with and
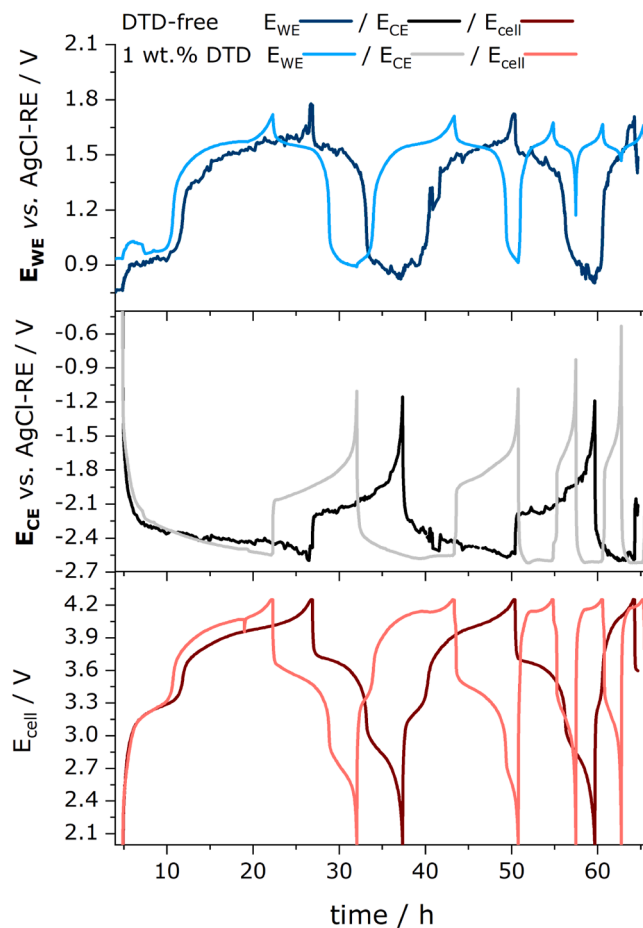

Fig. 7. 3-electrode experiments against a AgCl-RE in EC:DEC-based 750 mM KPF$_6$ electrolytes with and without DTD (1 wt.%) as electrolyte additive in KFF/AgCl-RE/graphite full cells. The top panel shows the working electrode (KFF) potential, E_{WE} vs. AgCl-RE; the middle panel displays the counter electrode (graphite) potential, E_{CE} vs. AgCl-RE. In the bottom panel the cell potential, E_{cell}, is plotted of the KFF/graphite full cell. The applied current corresponded to galvanostatic cycling rates of C/20 on the first two cycles, before the rate was increased to C/10 on the following cycles.

without DTD (Fig. 7, **top**) share the same 2-step profile that is consistent with the profiles shown above in Fig. 3b and Fig. 6a. This stresses our findings above that the excessive formation of DEDD at the potassium counter electrode plays an important role in the high degree of irreversible reactions during cycling and self-discharge under OCV. There is a 80 mV difference in the lower potential plateaus between the two cells (0.92 V (0 wt% DTD) and 1.00 V (1 wt% DTD) vs. AgCl-RE, which is in agreement with the CV experiments (Fig. 5). Already on the first cycle, the lower discharge potential is almost completely absent, which suggests high degrees of irreversible losses during charge at the negative electrode, e.g. due to SEI formation, as a main origin of loss of charge carrier inventory. In turn, the reduction reaction is limited by the remaining active charge carrier inventory.

When analyzing the Gr-CE potential profiles (Fig. 7, **middle**), it is readily seen that the main cause of the rapid capacity decay is rooted in the poor electrochemical behavior of the graphite electrode in presence of DTD (grey line), as already demonstrated in the discussion above (Fig. 6b). The potential in the DTD-containing cell shows no characteristic intercalation plateau, unlike the DTD-free standard electrolyte, and drops rapidly to low potentials until the cell's cut-off limit is reached. Interestingly, on the following cycles signs of K-plating are observed that appear as a constant potential section at −2.56 V vs. AgCl-RE. At the same time the end point potentials during discharge are

slipping, because the KFF electrode only retained the upper potential step. As the potential end point of KFF is shifting to higher potentials, the graphite end point potentials must shift as well until the cut-off (cell) voltage is reached. In contrast, the Gr-CE in the DTD-free cell (black line) shows the characteristic intercalation features and retains the charge carrier inventory better than the cell with DTD additive.

4. Discussion

Positive electrodes may suffer from crosstalk with electrolyte degradation products, such as DEDD [1,2,50] [ref]. Herein, we stressed the fact that KFF, as a commonly used positive electrode material in KIBs, showed high degrees of irreversible reactions, which is reflected in a long, 2-step potential profile in the high voltage region above 3.75 V vs. K^+/K. The CV experiments in Fig. 5 shows quite clearly the appearance of an additional feature on the anodic scan. Moreover, KFF/K-CE half cells enter a self-discharge process under OCV conditions that is induced by DEDD (and similar ethylene bis(alkyl dicarbonates)), as illustrated in Scheme 2. Even small amounts of K-metal can induce the formation of these compounds, which is why REs based on K-metal raise an issue in 3e full cell tests as well. This essentially disqualifies two commonly used approaches to perform 3e measurements in half and full cells [22,25], namely the use of metallic electrodes (here K-RE) and partly charged electrode materials with a flat potential region, which was explored herein with a KFF electrode. Moving away from K-RE seems particularly important, since the measured potential of the electrode appears to depend strongly on its preparation history and purity [13,31] Similar findings for the Na-ion system have been reported previously[22,25]and confirm our general conclusions herein.

Therefore, we herein proposed an alternative reference electrode, using Ag-wire in a saturated TBACl solution (AgCl-RE), which is placed in a separate glass capillary compartment (Scheme 1). The electrolyte solvent mixture can be adjusted as needed and referenced with respect to the ferrocene redox couple (Fc^+/Fc) to relate to other electrolyte compositions. This eliminates the problems associated with DEDD that is formed in the electrolyte in contact with K-metal. In this first generation, there are still minor setup-related issues, for example, the cell is not tightly sealed around the RE-compartment and thus has to be operated inside a glovebox. As a result, there is a small degree of solvent evaporation from the cell compartment that could affect long-term measurements. In addition, maintaining a constant contact pressure between the soaked separator in the cell compartment and the RE-capillary membrane was challenging, which might explain the voltage fluctuations encountered in some of the experiments. Our experiments highlight that the AgCl-RE based 3e setup enables unbiased measurements from degraded electrolyte species in the reactive KIB system. In this work, we have used this cell configuration to 1) understand the deterioration of the K-metal electrode and polarization effects, 2) study graphite/KFF cells without the detrimental influence of K-RE and 3) investigate the impact of DTD on the electrochemistry in half and full cells.

In this context, the self-discharge processes at the KFF electrode, induced by electrolyte degradation products formed at the K-metal electrode was outlined in a comparison of electrochemical responses from galvanostatic and cyclic voltammetry measurements in various 2e and 3e setups using either K-RE, KFF-RE or AgCl-RE. In this selection of reference electrodes the AgCl-RE was the only reference that would allow us to monitor both electrode sides individually and independent from both the choice of electrodes and electrolyte. This circumvents interferences in the electrode potential profiles from degradation products. As demonstrated throughout our experiments, the role of K-metal in terms of its actual redox-potential and polarization play a key role in accelerated degradation of half cell configurations and more importantly, may induce misleading artefacts and detrimental electrode processes. In accordance with previous findings by Hosaka et al. [20].
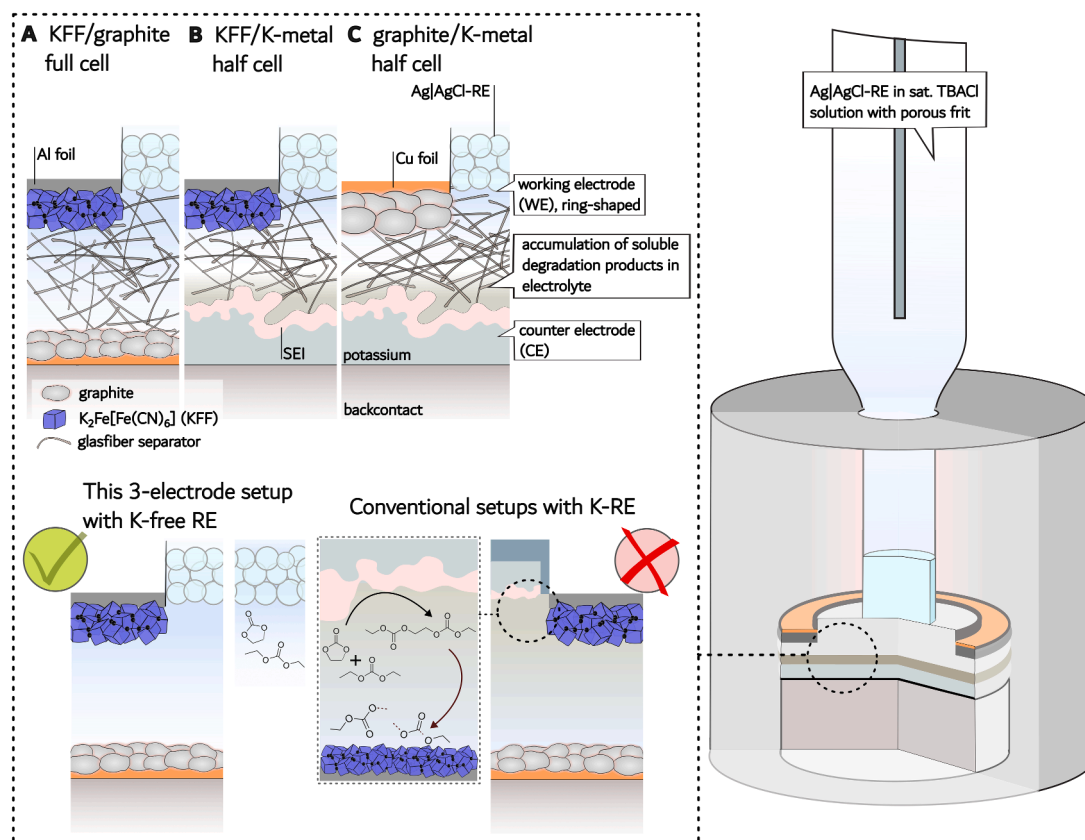
Scheme 2. Illustration of the cell setup and the cross-talk induced reactions at the negative and positive electrodes in K-ion batteries due to the formation of ethylene bis(alkyl dicarbonates) at the reactive potassium counter or reference electrode.

and Ko et al. [48,49], the 3e measurements showed that the effect of DTD on the graphite electrode are two-fold: In K/graphite half cells it was observed that the redox potential of the K-metal electrode shifts to more positive values. As a result, the cell voltage between Gr-WE and K-CE narrows and therefore Gr-WE approaches the lower cut-off limit prematurely. The origin of this behavior is not completely clear, as the formation of more passivating layers would change the overpotential around the equilibrium potential of potassium (kinetic effect). It is also observed only when an oxidative current is applied first. On the other hand, potential drifts of reactive alkali metals are quite common observed[22] and large deviations of hundreds of mV in K/K symmetrical cells have been reported after assembly[13,18]. Such marked potential differences are a particular issue with potassium metal. In graphite/KFF full cells it was further seen that DTD takes part in the degradation of graphite, as the characteristic intercalation signatures could not be observed. In addition, from the second cycle onwards, signs of K-plating were observed.

5. Conclusion

Reference electrodes (REs) should be independent of the electrolyte formulation or provide a means to compare them with one another. Furthermore, they should not interfere with the electrode process, while maintaining a constant potential over a long period of time. The thin layer setups used in battery research make it often difficult to implement a suitable RE. In this work we have outlined, why the choice of a suitable RE is particularly challenging for KIB systems. Because of the fast degradation of K-metal, its strong dependence on the preparation history and material grade poses a lot of problems. For instance, K-metal as counter (K-CE) or reference (K-RE) electrode induces strong crosstalk with severe degrees of irreversible reactions on the first cycles, as well as a strong self-discharge when stored under OCV conditions. Therefore, we explored herein a first generation 3-electrode setup with a RE based on Ag-wire in a saturated TBACl solution (AgCl-RE). The corresponding cell configuration allows the introduction of silver-based RE in a separated counterpart while maintaining the geometry of the coin cell battery and utilising a separator that is a few hundred microns thick, thereby reducing the electrolyte volume. Furthermore, it can be employed independently of the cell chemistry and can be readily adapted to the respective electrolyte formulation.

To demonstrate its use, the impact of the electrolyte additive DTD was investigated in half and full cells, to show its effects on the electrochemical processes at the K-metal, KFF and graphite electrodes. While the setup will need further improvements in the future, we believe that the general approach to move the RE into a separate cell compartment is promising and a viable strategy to minimize interferences between RE and other cell components.

Declaration of generative AI and AI-assisted technologies in the writing process

During the preparation of this work the author(s) used *DeepL Write* in order to improve language and readability. After using this tool/service, the authors reviewed and edited the content as needed and take full responsibility for the content of the publication.

CRediT authorship contribution statement

Iurii Panasenko: Writing – review & editing, Writing – original draft, Validation, Methodology, Investigation, Formal analysis, Data curation. **Monika Bäuerle:** Writing – review & editing, Supervision, Methodology, Conceptualization. **Fabian Jeschull:** Writing – review & editing, Supervision, Project administration, Funding acquisition, Conceptualization.

Declaration of competing interest

The authors declare the following financial interests/personal relationships which may be considered as potential competing interests:

Fabian Jeschull reports financial support was provided by German Research Foundation. If there are other authors, they declare that they have no known competing financial interests or personal relationships that could have appeared to influence the work reported in this paper.

Data availability statement

The data to the above presented findings are available on Zenodo online repository DOI: 10.5281/zenodo.12205268 (ref [51]).

Acknowledgements

Supplementary materials

Supplementary material associated with this article can be found, in the online version, at doi:10.1016/j.electacta.2024.145551.

Data availability

We have uploaded our data on Zenodo and generated a DOI, which we included as reference in this manuscript. The data will be made available upon acceptance of this manuscript.

References

[1] A. Hofmann, F. Müller, S. Schöner, F. Jeschull, Revealing the formation of dialkyl dioxahexane dioate products from ethylene carbonate based electrolytes on lithium and potassium surfaces, Batter. Supercaps (2023) e202300325, https://doi.org/10.1002/batt.202300325.

[2] L. Caracciolo, L. Madec, G. Gachot, H. Martinez, Impact of the salt anion on K metal reactivity in EC/DEC studied using GC and XPS analysis, ACS Appl. Mater. Interfaces 13 (2021) 57505–57513, https://doi.org/10.1021/acsami.1c19537.

[3] T. Hosaka, T. Fukabori, T. Matsuyama, R. Tatara, K. Kubota, S. Komaba, 1,3,2-Dioxathiolane 2,2-Dioxide as an electrolyte additive for K-Metal cells, ACS Energy Lett 6 (2021) 3643–3649, https://doi.org/10.1021/acsenergylett.1c01238.

[4] F. Allgayer, J. Maibach, F. Jeschull, Comparing the solid electrolyte interphases on graphite electrodes in K and li half cells, ACS Appl. Energy Mater. 5 (2022) 1136–1148, https://doi.org/10.1021/acsaem.1c03491.

[5] A.J. Naylor, M. Carboni, M. Valvo, R. Younesi, Interfacial reaction mechanisms on graphite anodes for K-Ion batteries, ACS Appl. Mater. Interfaces 11 (2019) 45636–45645, https://doi.org/10.1021/acsami.9b15453.

[6] S. Xing, A. Khudyshkina, U.-C. Rauska, A.J. Butzelaar, D. Voll, P. Theato, J. Tübke, F. Jeschull, Degradation of styrene-Poly(ethylene oxide)-Based block copolymer electrolytes at the Na and K negative electrode studied by microcalorimetry and impedance spectroscopy, J. Electrochem. Soc. 171 (2024) 040516, https://doi.org/10.1149/1945-7111/ad3b72.

[7] F. Jeschull, J. Maibach, Inactive materials matter: how binder amounts affect the cycle life of graphite electrodes in potassium-ion batteries, Electrochem. Commun. 121 (2020) 106874, https://doi.org/10.1016/j.elecom.2020.106874.

[8] B. Larhrib, L. Madec, Toward highly reliable potassium-ion half and full coin cells, Batter. Supercaps 6 (2023) e202300061, https://doi.org/10.1002/batt.202300061.

[9] M. Fiore, S. Wheeler, K. Hurlbutt, I. Capone, J. Fawdon, R. Ruffo, M. Pasta, Paving the way toward highly efficient, high-energy potassium-ion batteries with ionic liquid electrolytes, Chem. Mater. 32 (2020) 7653–7661, https://doi.org/10.1021/acs.chemmater.0c01347.

[10] X. Bie, K. Kubota, T. Hosaka, K. Chihara, S. Komaba, A novel K-ion battery: hexacyanoferrate(II)/graphite cell, J. Mater. Chem. A 5 (2017) 4325–4330, https://doi.org/10.1039/C7TA00220C.

[11] C. Müller, Z. Wang, A. Hofmann, P. Stüble, X. Liu-Théato, J. Klemens, A. Smith, Influences on reliable capacity measurements of hard carbon in highly loaded electrodes, Batter. Supercaps 6 (2023) e202300322, https://doi.org/10.1002/batt.202300322.

[12] C. Bünzli, H. Kaiser, P. Novák, Important aspects for reliable electrochemical impedance spectroscopy measurements of li-ion battery electrodes, J. Electrochem. Soc. 162 (2015) A218–A222, https://doi.org/10.1149/2.1061501jes.

[13] T. Hosaka, S. Muratsubaki, K. Kubota, H. Onuma, S. Komaba, Potassium metal as reliable reference electrodes of nonaqueous potassium cells, J. Phys. Chem. Lett. 10 (2019) 3296–3300, https://doi.org/10.1021/acs.jpclett.9b00711.

[14] B.E. Murdock, C.G. Armstrong, D.E. Smith, N. Tapia-Ruiz, K.E. Toghill, Misreported non-aqueous reference potentials: the battery research endemic, Joule 6 (2022) 928–934, https://doi.org/10.1016/j.joule.2022.04.009.

[15] J. Hou, R. Girod, N. Nianias, T.-H. Shen, J. Fan, V. Tileli, Lithium-gold reference electrode for potential stability during in situ electron microscopy studies of lithium-ion batteries, J. Electrochem. Soc. 167 (2020) 110515, https://doi.org/10.1149/1945-7111/ab9eea.

[16] Y.-C. Chien, D. Brandell, M.J. Lacey, Towards reliable three-electrode cells for lithium–sulfur batteries, Chem. Commun. 58 (2022) 705–708, https://doi.org/10.1039/D1CC04553A.

[17] J. Landesfeind, H.A. Gasteiger, Temperature and concentration dependence of the ionic transport properties of lithium-ion battery electrolytes, J. Electrochem. Soc. 166 (2019) A3079, https://doi.org/10.1149/2.0571912jes.

[18] B. Jagger, J. Aspinall, S. Kotadi, J. Cattermull, S. Dhir, M. Pasta, Potassium alloy reference electrodes for potassium-ion batteries: the K-In and K-Bi systems, ACS Mater. Lett. (2024) 4498–4506, https://doi.org/10.1021/acsmaterialslett.4c01219.

[19] S. Yi, B. Wang, Z. Chen, R. Wang, D. Wang, A study on LiFePO$_4$/graphite cells with built-in Li$_4$Ti$_5$O$_{12}$ reference electrodes, RSC Adv 8 (2018) 18597–18603, https://doi.org/10.1039/C8RA03062F.

[20] T. Hosaka, T. Matsuyama, R. Tatara, Z.T. Gossage, S. Komaba, Impact of electrolyte decomposition products on the electrochemical performance of 4 V class K-ion batteries, Chem. Sci. 14 (2023) 8860–8868, https://doi.org/10.1039/D3SC02111D.

[21] M.J. Trahan, S. Mukerjee, E.J. Plichta, M.A. Hendrickson, K.M. Abraham, Studies of Li-Air cells utilizing dimethyl sulfoxide-based electrolyte, J. Electrochem. Soc. 160 (2012) A259, https://doi.org/10.1149/2.048302jes.

[22] S.E. Lee, M.H. Tang, Reliable reference electrodes for nonaqueous sodium-ion batteries, J. Electrochem. Soc. 166 (2019) A3260, https://doi.org/10.1149/2.0401914jes.

[23] Y. Lyu, P. Mollik, A.L. Oláh, D.P. Halter, Construction and evaluation of cheap and robust miniature Ag/AgCl reference electrodes for aqueous and organic electrolytes, Chem. Electro. Chem. 11 (2024) e202300792, https://doi.org/10.1002/celc.202300792.

[24] E.C. Cengiz, J. Rizell, M. Sadd, A. Matic, N. Mozhzhukhina, Review—reference electrodes in li-ion and next generation batteries: correct potential assessment, applications and practices, J. Electrochem. Soc. 168 (2021) 120539, https://doi.org/10.1149/1945-7111/ac429b.

[25] S.E. Lee, M.H. Tang, Electroactive decomposition products cause erroneous intercalation signals in sodium-ion batteries, Electrochem. Commun. 100 (2019) 70–73, https://doi.org/10.1016/j.elecom.2019.01.024.

[26] Polarography and voltammetry in non-aqueous solutions, Electrochem. Nonaqueous Solut. (2002) 223–267, https://doi.org/10.1002/3527600655.ch8.

[27] A.A.J Torriero, Understanding the differences between a quasi-reference electrode and a reference electrode, Med. Anal. Chem. Int. J. (2019) 3, https://doi.org/10.23880/MACIJ-16000144.

[28] L. Madec, V. Gabaudan, G. Gachot, L. Stievano, L. Monconduit, H. Martinez, Paving the way for K-Ion batteries: role of electrolyte reactivity through the example of sb-based electrodes, ACS Appl. Mater. Interfaces 10 (2018) 34116–34122, https://doi.org/10.1021/acsami.8b08902.

[29] A.D. Khudyshkina, P.A. Morozova, A.J. Butzelaar, M. Hoffmann, M. Wilhelm, P. Theato, S.S. Fedotov, F. Jeschull, Poly(ethylene oxide)-based electrolytes for solid-state potassium metal batteries with a prussian blue positive electrode, ACS Appl. Polym. Mater. 4 (2022) 2734–2746, https://doi.org/10.1021/acsapm.2c00014.

[30] F. Holtstiege, A. Wilken, M. Winter, T. Placke, Running out of lithium? A route to differentiate between capacity losses and active lithium losses in lithium-ion batteries, Phys. Chem. Chem. Phys. 19 (2017) 25905–25918, https://doi.org/10.1039/C7CP05405J.

[31] S. Dhir, B. Jagger, A. Maguire, M. Pasta, Fundamental investigations on the ionic transport and thermodynamic properties of non-aqueous potassium-ion electrolytes, Nat. Commun. 14 (2023) 3833, https://doi.org/10.1038/s41467-023-39523-0.

[32] J. Rizell, W. Chrobak, N. Mozhzhukhina, S. Xiong, A. Matic, Electrochemical signatures of potassium plating and stripping, J. Electrochem. Soc. 171 (2024) 020517, https://doi.org/10.1149/1945-7111/ad2593.

[33] J. Zhao, X. Zou, Y. Zhu, Y. Xu, C. Wang, Electrochemical intercalation of potassium into graphite, Adv. Funct. Mater. 26 (2016) 8103–8110, https://doi.org/10.1002/adfm.201602248.

[34] H. Onuma, K. Kubota, S. Muratsubaki, W. Ota, M. Shishkin, H. Sato, K. Yamashita, S. Yasuno, S. Komaba, Phase evolution of electrochemically potassium intercalated graphite, J. Mater. Chem. A 9 (2021) 11187–11200, https://doi.org/10.1039/D0TA12607A.

[35] F. La Mantia, C.D. Wessells, H.D. Deshazer, Y. Cui, Reliable reference electrodes for lithium-ion batteries, Electrochem. Commun. 31 (2013) 141–144, https://doi.org/10.1016/j.elecom.2013.03.015.

[36] F. Jeschull, D. Brandell, K. Edström, M.J. Lacey, A stable graphite negative electrode for the lithium–sulfur battery, Chem. Commun. 51 (2015) 17100–17103, https://doi.org/10.1039/C5CC06666B.

[37] M.J. Lacey, F. Jeschull, K. Edström, D. Brandell, Functional, water-soluble binders for improved capacity and stability of lithium–sulfur batteries, J. Power Sources 264 (2014) 8–14, https://doi.org/10.1016/j.jpowsour.2014.04.090.

[38] R. Mogensen, D. Brandell, R. Younesi, Solubility of the solid electrolyte interphase (SEI) in sodium ion batteries, ACS Energy Lett 1 (2016) 1173–1178, https://doi.org/10.1021/acsenergylett.6b00491.

[39] Y. Mo, W. Zhou, K. Wang, K. Xiao, Y. Chen, Z. Wang, P. Tang, P. Xiao, Y. Gong, S. Chen, P. Gao, J. Liu, Engineering electrode/electrolyte interphase chemistry toward high-rate and long-life potassium ion full-cell, ACS Energy Lett 8 (2023) 995–1002, https://doi.org/10.1021/acsenergylett.2c02659.

[40] K.R. Cho, M. Kim, B. Kim, G. Shin, S. Lee, W. Kim, Investigation of the AgCl formation mechanism on the ag wire surface for the fabrication of a marine low-frequency-electric-field-detection Ag/AgCl sensor electrode, ACS Omega 7 (2022) 25110–25121, https://doi.org/10.1021/acsomega.2c01481.

[41] Y. Marcus, Thermodynamic functions of transfer of single ions from water to nonaqueous and mixed solvents: part 3 - Standard potentials of selected electrodes, 57 (1985) 1129–1132. https://doi.org/10.1351/pac198557081129.

[42] N. Matsuura, K. Umemoto, Z. Takeuchi, Standard potentials of alkali metals, silver, and thallium Metal/Ion couples in N,N′-Dimethylformamide, dimethyl sulfoxide, and propylene carbonate, Bull. Chem. Soc. Jpn. 47 (1974) 813–817, https://doi.org/10.1246/bcsj.47.813.

[43] S. Komaba, T. Hasegawa, M. Dahbi, K. Kubota, Potassium intercalation into graphite to realize high-voltage/high-power potassium-ion batteries and potassium-ion capacitors, Electrochem. Commun. 60 (2015) 172–175, https://doi.org/10.1016/j.elecom.2015.09.002.

[44] A.W. Ells, R. May, L.E. Marbella, Potassium fluoride and carbonate lead to cell failure in potassium-ion batteries, ACS Appl. Mater. Interfaces 13 (2021) 53841–53849, https://doi.org/10.1021/acsami.1c15174.

[45] Y. Feng, A.M. Rao, J. Zhou, B. Lu, Selective potassium deposition enables dendrite-resistant anodes for ultrastable potassium-metal batteries, Adv. Mater. 35 (2023) 2300886, https://doi.org/10.1002/adma.202300886.

[46] M. Hamada, R. Tatara, K. Kubota, S. Kumakura, S. Komaba, All-solid-state potassium polymer batteries enabled by the effective pretreatment of potassium metal, ACS Energy Lett 7 (2022) 2244–2246, https://doi.org/10.1021/acsenergylett.2c01096.

[47] J. Zhao, B. Jagger, L.F. Olbrich, J. Ihli, S. Dhir, M. Zyskin, X. Ma, M. Pasta, Transport and thermodynamic properties of KFSI in TEP by operando raman gradient analysis, ACS Energy Lett 9 (2024) 1537–1544, https://doi.org/10.1021/acsenergylett.4c00661.

[48] S. Ko, X. Han, T. Shimada, N. Takenaka, Y. Yamada, A. Yamada, Electrolyte design for lithium-ion batteries with a cobalt-free cathode and silicon oxide anode, Nat. Sustain. (2023), https://doi.org/10.1038/s41893-023-01237-y.

[49] S. Ko, T. Obukata, T. Shimada, N. Takenaka, M. Nakayama, A. Yamada, Y. Yamada, Electrode potential influences the reversibility of lithium-metal anodes, Nat. Energy 7 (2022) 1217–1224, https://doi.org/10.1038/s41560-022-01144-0.

[50] G.G. Eshetu, S. Grugeon, H. Kim, S. Jeong, L. Wu, G. Gachot, S. Laruelle, M. Armand, S. Passerini, Comprehensive Insights into the Reactivity of Electrolytes Based on Sodium Ions, ChemSusChem 9 (2016) 462–471, https://doi.org/10.1002/cssc.201501605.

[51] I. Panasenko, F. Jeschull, M. Bäuerle, Supporting data for "How Reference Electrodes Improve Our Understanding of Degradation Processes in Half- and Full-Cell Cell Potassium-Ion Battery Setups" [Data set]., (2024). https://doi.org/10.5281/zenodo.12205268.